

Article

A Deep Learning Framework for Adaptive Beamforming in Massive MIMO Millimeter Wave 5G Multicellular Networks

Spyros Lavdas ^{1,*}, Panagiotis K. Gkonis ², Efthalia Tsaknaki ¹, Lambros Sarakis ², Panagiotis Trakadas ³ and Konstantinos Papadopoulos ²

¹ Department of Computer Science, Neapolis University, 8042 Pafos, Cyprus; e.tsaknaki.1@nup.ac.cy

² Department of Digital Industry Technologies, National and Kapodistrian University of Athens,

34400 Dirfies Messapies, Greece; pgkonis@dind.uoa.gr (P.K.G.); lsarakis@uoa.gr (L.S.); konspap@uoa.gr (K.P.)

³ Department of Port Management and Shipping, National and Kapodistrian University of Athens,

34400 Dirfies Messapies, Greece; ptrakadas@pms.uoa.gr

* Correspondence: s.lavdas@nup.ac.cy

Abstract: The goal of this paper is the performance evaluation of a deep learning approach when deployed in fifth-generation (5G) millimeter wave (mmWave) multicellular networks. To this end, the optimum beamforming configuration is defined by two neural networks (NNs) that are properly trained, according to mean square error (MSE) minimization. The first network has as input the requested spectral efficiency (SE) per active sector, while the second network has the corresponding energy efficiency (EE). Hence, channel and power variations can now be taken into consideration during adaptive beamforming. The performance of the proposed approach is evaluated with the help of a developed system-level simulator via extensive Monte Carlo simulations. According to the presented results, machine learning (ML)-adaptive beamforming can significantly improve EE compared to the standard non-ML framework. Although this improvement comes at the cost of increased blocking probability (BP) and radiating elements (REs) for high data rate services, the corresponding increase ratios are significantly reduced compared to the EE improvement ratio. In particular, considering 21.6 Mbps per active user and ML adaptive beamforming, the EE can reach up to 5.3 Mbps/W, which is significantly improved compared to the non-ML case (0.9 Mbps/W). In this context, BP does not exceed 2.6%, which is slightly worse compared to 1.7% in the standard non-ML case. Moreover, approximately 20% additional REs are required with respect to the non-ML framework.

Keywords: 5G; mmWave; massive MIMO; machine learning; adaptive beamforming; system level simulations



Citation: Lavdas, S.; Gkonis, P.K.; Tsaknaki, E.; Sarakis, L.; Trakadas, P.; Papadopoulos, K. A Deep Learning Framework for Adaptive Beamforming in Massive MIMO Millimeter Wave 5G Multicellular Networks. *Electronics* **2023**, *12*, 3555. <https://doi.org/10.3390/electronics12173555>

Academic Editor: Ikmo Park

Received: 26 July 2023

Revised: 14 August 2023

Accepted: 21 August 2023

Published: 23 August 2023



Copyright: © 2023 by the authors. Licensee MDPI, Basel, Switzerland. This article is an open access article distributed under the terms and conditions of the Creative Commons Attribution (CC BY) license (<https://creativecommons.org/licenses/by/4.0/>).

1. Introduction

The full deployment of fifth-generation (5G) broadband wireless cellular networks has enabled the transition toward advanced features and applications, such as enhanced mobile broadband (eMBB), ultra-reliable low latency communications (URLLC) as well as massive machine-type communications (mMTC) [1,2]. To this end, various novel technologies have been introduced in the physical layer, such as millimeter-wave (mmWave) transmission [3], non-orthogonal multiple access (NOMA) [4] as well as massive multiple input multiple output (m-MIMO) configurations [5]. Moreover, as the discussions on the next generation of wireless networks (sixth generation, 6G) have already started taking place [6], network densification is leveraged as an efficient way to provide seamless connectivity to a vast number of mobile devices. In this context, the single link concept (i.e., base station (BS) to mobile station (MS)) is replaced by various potential links from access points (APs) and relay nodes.

However, traditional m-MIMO relies on large-scale phase arrays, which induce high hardware cost and power consumption due to the energy consuming phase shifters, especially when the number of antennas grows. Additionally, the transmitted signal inevitably

interacts with the surrounding objects, thereby degrading the signal-to-noise ratio (SNR) and quality of service (QoS). To this end, the burgeoning Intelligent Reflective Surface (IRS) technology that has recently emerged constitutes a state-of-the-art reflective beamformer with extremely low complexity and low hardware expenditure [7]. The IRS technology is based on the concept of metasurfaces, which consist of passive sub-wavelength reflecting elements whose electromagnetic behavior can be easily altered through electronic devices such as positive-intrinsic-negative (PIN) diodes or micro-electromechanical system (MEMS). In this context, the power-hungry phase shifters are replaced by the former low-cost electronic devices. In addition, the appropriate position of IRSs facilitates the bypass of the environmental obstacles along the signal propagation. Thus, the detrimental effects of signal attenuation and scattering can be potentially mitigated. Even though there are promising results in indoor applications [8], IRS technology is relatively limited in m-MIMO cellular networks as there are still open research issues to tackle such as the deployment of IRS in a hybrid wireless network with multiple BSs and the exploration of its optimal position and orientation in a given cellular network [9,10].

As may be seen from the preceding, in next-generation wireless networks, a significantly large number of antennas will be deployed per AP. Hence, appropriate beamforming algorithms should be configured that not only ensure uninterrupted connectivity but also minimize interference levels. In this paper, we deal with a computationally efficient adaptive beamforming technique in multicellular mmWave m-MIMO orientations. In this case, the goal is to improve various key performance indicators (KPIs), such as energy efficiency (EE) and spectral efficiency (SE). In general, adaptive beamforming in 5G orientations has attracted scientific research interest over the last years. In this context, in [11], the performance of various precoding schemes is evaluated with an emphasis on hybrid beamforming, which is a challenging beamforming approach that is based on the use of fewer active radio-frequency (RF) chains compared to the total number of antennas. According to the presented results, hybrid precoding methods can improve the sum rate and SE. In particular, one of the main effective hybrid precoders proposed in the literature of m-MIMO beamforming schemes is phased-zero-forcing (PZF), which improves the SNR and SE. However, ref. [12] manifests that PZF beamforming needs further improvement in densely deployed networks. In the same context of m-MIMO beamforming, the provided simulations in [13] suggest a higher number of parallel data streams per user in a mmWave system to achieve higher-order throughputs. Interestingly enough, it has been demonstrated that the need for active antenna elements decreases with the number of parallel data streams. In [14], the performance of a cooperative hybrid beamforming method is evaluated that is based on the sum-utility maximization. According to the presented results, the proposed method has similar performance compared to fully digital beamforming even when operated with practical finite-resolution phase shifters. In [15], the concept of ultra-dense cell-free m-MIMO systems for sustainable 6G wireless communications is introduced. The key findings of the work conclude that the support of high data rates requires a holistic network redesign to maximize EE (dense deployment, green design, etc.). In a similar cell-free m-MIMO system, ref. [16] proposes an optimum beamforming scheme which outperforms zero-forcing and conjugate beamforming. Even though the former work can achieve beamforming and power control, it significantly increases the system's complexity. In [17], the performance of the least mean square (LMS) algorithm is investigated in the context of 5G-MIMO configurations. To this end, several optimization algorithms are evaluated under various parameters (i.e., antenna elements, antenna spacing, etc.).

The coexistence of various novel technologies in the physical layer of the next-generation broadband wireless networks as it was previously mentioned, along with increased user traffic and mobility patterns, creates a multiparameter environment with various constraints. Hence, traditional optimization algorithms on one hand would have to search over multidimensional spaces for potential solutions, and on the other hand, the optimization process would have to be repeated over regular time intervals (e.g., coherence time). Therefore, latency minimization, which is a key concept in 5G/6G networks, would

not be always satisfied. Over the last few years, machine learning (ML) algorithms have emerged as a promising solution that can deal with a variety of optimization problems. In general, ML algorithms can be classified into three major categories [18–20]: supervised learning (SL) where training is based on well-known datasets, unsupervised learning, where there is no data pattern, as well as reinforcement learning (RL). In the latter case, a mobile agent interacts with the environment to define the best possible action per case.

In the ML framework, a survey of the most important approaches categorized per m-MIMO application (i.e., channel estimation, signal detection, hybrid beamforming, coexistence with NOMA, etc.) is provided in [21]. In [22], a novel deep reinforcement learning (DRL)-based coordinated beamforming scheme has been considered, where a single MS can be served by multiple BSs. In this context, the goal is to derive suboptimal beamforming vectors at BSs out of possible beamforming codebook candidates. The beamforming vectors are chosen according to sum rate maximization. In [23], the concept of federated learning (FL) in m-MIMO configurations is introduced to optimize various metrics, such as MS assignments and transmission powers. To this end, ML-aided resource optimization is performed in a decentralized way in discrete time intervals. In [24], an SL approach is considered for user positioning that can outperform other ML schemes such as the k -nearest neighbors (k -NN) algorithm and support vector machines (SVMs). In [25], a deep learning (DL) approach is presented to simplify the process of estimating beamforming weights. According to the presented results, the proposed approach can significantly reduce the overall complexity in weight estimation. In [26], hybrid beamforming is used for EE maximization. In the same context, a low-complexity method that is based on adaptive cross-entropy (ACE)-based optimization with low-bit phase shifters was proposed in order to handle the sum rate maximization problem. In [27], the authors present an approach based on a convolutional neural network (CNN) structure, namely WBPNet, to realize adaptive time-domain wideband beamforming without delay structures under insufficient snapshots. In [28], a DL-NN is proposed for hybrid precoders and combiners to improve spectral efficiency. A key advantage of the proposed approach is that it does not require prior knowledge such as angle features and channel information. In [29], the authors evaluate the performance of an adaptive beamforming approach in 5G multicellular mmWave orientations with the help of a k -NN SL method that selects the appropriate beamforming configuration based on the requested SE in an active sector. According to the presented results, this approach provides similar SE and EE levels when compared to the conventional non-ML approach, at the cost however of increased BP.

The goal of the study presented in this paper is to extend the work in [29] and investigate the performance of a DL approach when deployed in 5G multicellular wireless orientations. To this end, the algorithm is trained with the help of a predefined number of samples to define the optimum positions of the generated beams. A key novelty of the proposed approach is that two NNs are now considered: one for SE and one for EE maximization. Hence, channel state information (CSI) knowledge can now be exploited during NN training in order to capture channel and power variations. As it will be discussed in the Results section, the proposed approach can significantly improve the EE for high data rate services compared to the standard non-ML approach with minimum increases in BP and the number of REs.

The rest of this paper is organized as follows: In Section 2, the multicellular orientation is described, while the deployed antenna configuration per BS sector is described in Section 3. In Section 4, the proposed ML adaptive beamforming framework is analyzed. In Section 5, the overall simulation setup is presented along with simulation results. Finally, concluding remarks are outlined in Section 6.

The following notation is used in the paper. An italic variable a denotes a scalar, whereas boldface lowercase and uppercase variables \mathbf{a} and \mathbf{A} denote vectors and matrices, respectively. Finally, a calligraphic \mathcal{A} denotes a set of $|\mathcal{A}|$ elements and notation $x:y$ denotes all elements from x to y with step 1.

2. Multicellular Orientation

We consider a multicellular orientation where MSs enter the network sequentially. At a given state in an arbitrary BS, the MSs follow a specific spatial distribution. According to this distribution, the appropriate beamforming configuration (BC) is selected based on the minimization of total downlink transmission power. Hence, the state per BS's sector is defined by the set $\{\mathbf{S}_{b,s}, \text{BC}(b,s)\}$, where $\mathbf{S}_{b,s}$ is an 1×180 vector matrix where non-zero entries indicate either the requested SE or EE in the corresponding angles. In the same context, $\text{BC}(b,s)$ indicates the BC in the s th sector of the b th BS ($1 \leq s \leq 3, 1 \leq b \leq B$). The overall geometry is depicted in Figure 1 for two tiers of cells around the central cell (19 cells in total). As it can be observed, there are three antenna configurations per BS located at the boundaries of the hexagonal cell, each covering an azimuth space of 180° . More details on the deployed antenna configuration per sector will be provided in the following section.

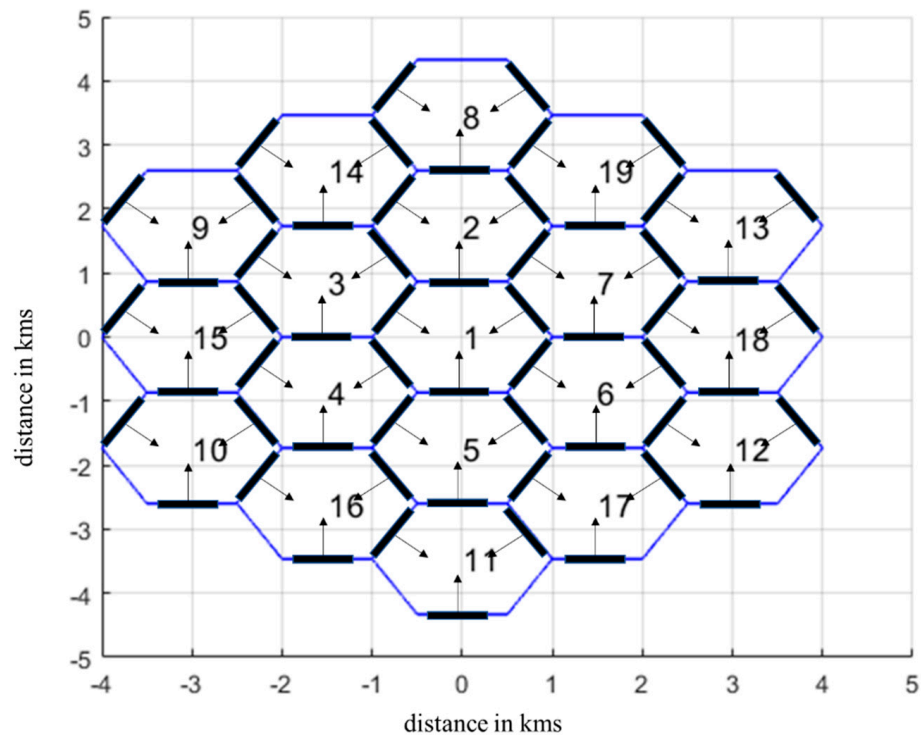


Figure 1. Multicellular mm-Wave m-MIMO orientation.

In 3GPP-channel modeling, a three-model representation of the MIMO channel is considered [30]. To this end, the wireless channel in the 5G air interface for a non-line of sight (NLOS) environment can be modeled as follows:

$$H_{u,q,n,m}^{\text{NLOS}} = \sqrt{\frac{P_n}{M}} \mathbf{F}_{rx,n,m}^T \mathbf{\Theta}_{n,m} \mathbf{F}_{tx,n,m} \exp\left(\frac{j2\pi(\hat{r}_{rx,n,m}^T \cdot \bar{d}_{rx,u})}{\lambda_o}\right) \exp\left(\frac{j2\pi(\hat{r}_{tx,n,m}^T \cdot \bar{d}_{tx,q})}{\lambda_o}\right) \quad (1)$$

$$H_{u,q,n}^{\text{NLOS}} = \sum_{m=1}^M H_{u,q,n,m}^{\text{NLOS}} \quad (2)$$

In this context, the channel coefficient between an arbitrary pair of tx-rx is decomposed to an equivalent number of channel coefficients from N clusters. The channel in each cluster is further decomposed to M subpaths. In (1), P_n represents the power of the n th cluster, $\mathbf{\Theta}_{n,m}$ is a 2×2 matrix with initial phases uniformly distributed in $(-\pi, \pi)$, and vector matrices $\mathbf{F}_{tx,n,m} / \mathbf{F}_{rx,n,m}$ represent the

field pattern of transmitting/receiving antenna element q/u , respectively ($1 \leq q \leq M_t, 1 \leq u \leq M_r$), for the m th subpath of the n th cluster. In particular:

$$\mathbf{F}_{rx,n,m} = \begin{bmatrix} F_{rx,u,\theta}(\theta_{n,m,ZoA}, \phi_{n,m,AoA}) \\ F_{rx,u,\phi}(\theta_{n,m,ZoA}, \phi_{n,m,AoA}) \end{bmatrix} \quad (3)$$

$$\mathbf{F}_{tx,n,m} = \begin{bmatrix} F_{tx,s,\theta}(\theta_{n,m,ZoD}, \phi_{n,m,AoD}) \\ F_{tx,s,\phi}(\theta_{n,m,ZoD}, \phi_{n,m,AoD}) \end{bmatrix} \quad (4)$$

$$\mathbf{\Theta}_{n,m} = \begin{bmatrix} \exp(j\Phi_{n,m}^{\theta\theta}) & \sqrt{\kappa_{n,m}^{-1}} \exp(j\Phi_{n,m}^{\theta\phi}) \\ \sqrt{\kappa_{n,m}^{-1}} \exp(j\Phi_{n,m}^{\phi\theta}) & \exp(j\Phi_{n,m}^{\phi\phi}) \end{bmatrix} \quad (5)$$

In (3) and (4), $\theta_{n,m,ZoD}$ and $\theta_{n,m,ZoA}$ represent the angles of departure (AoD) and arrival (AoA), respectively, in the vertical plane for the m th subpath ($1 \leq m \leq M$) of the n th cluster ($1 \leq n \leq N$). The corresponding parameters for the horizontal plane are $\phi_{n,m,AoD}$ and $\phi_{n,m,AoA}$, respectively. Moreover, set $\{\Phi_{n,m}^{\theta\theta}, \Phi_{n,m}^{\theta\phi}, \Phi_{n,m}^{\phi\theta}, \Phi_{n,m}^{\phi\phi}\}$ in (5) corresponds to initial phases uniformly distributed in $(-\pi, \pi)$ as previously mentioned, while the $\kappa_{n,m}$ parameter is the generated cross-polarization power ratio (XPR) for each ray m of cluster n . Moreover, $\bar{d}_{rx,u}/\bar{d}_{tx,u}$ is the location vector of receive/transmit antenna element u/q , respectively, and λ_o is the carrier wavelength. Finally, $\hat{r}_{rx,n,m}$ and $\hat{r}_{tx,n,m}$ are the spherical unit vectors.

The corresponding geometry (considering only the x-y plane) is depicted in Figure 2, where Ω_{BS}/Ω_{MS} denote the orientation of the BS/MS antenna array, respectively, which is defined as the difference between the broadside of the BS/MS array and the absolute north (N) reference direction. Moreover, θ_{BS} is the line of sight (LOS) AoD direction between the BS and MS (with respect to the broadside of the BS array), while θ_{MS} is the AoA between the BS-MS LOS and the MS broadside. Finally, $\Delta_{n,m,AoD}$ is the angle offset of the m th subpath with respect to $\theta_{n,m,AoD}$ and $\Delta_{n,m,AoA}$ the corresponding offset with respect to $\theta_{n,m,AoA}$.

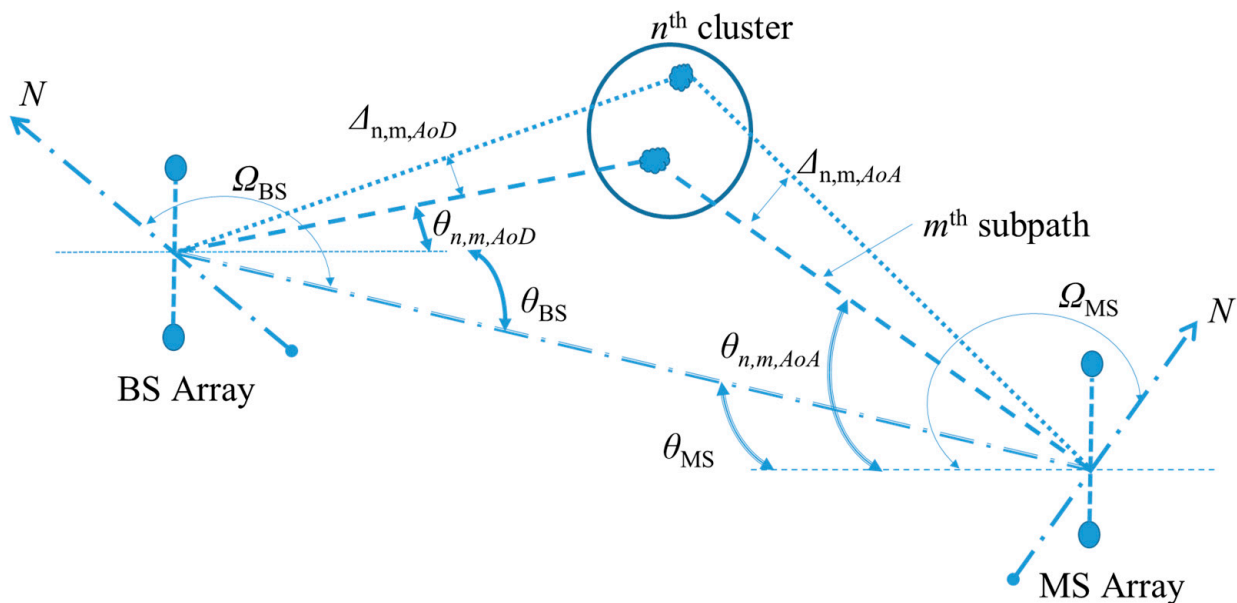


Figure 2. Clusters and subpaths in 3GPP channel modeling.

3. Proposed Antenna Design

The employed antenna array configuration scheme of the current work is characterized by low-cost fabrication in an effort to reduce hardware complexity. In particular, the suggested mmWave antenna configuration consists of a 21×21 array of rounded crossed bowtie radiating elements (REs) as shown in Figure 3. In order to achieve a unidirectional radiation pattern with the minimum waste of energy through the back lobe, two ground planes have been located below each RE at a distance of $\lambda_o/4$ and $\lambda_o/2$, respectively, with reference to each rounded bowtie antenna, as shown in the right panel of Figure 3 [31]. It should be noted at this point that the crossed rounded bowtie antennas, used as the exciter of the reflector, have been rotated at $\pm 45^\circ$ to enhance the formula-

tion of an adaptive dual-polarized radiation pattern [32], which is a critical property for cellular network communications.

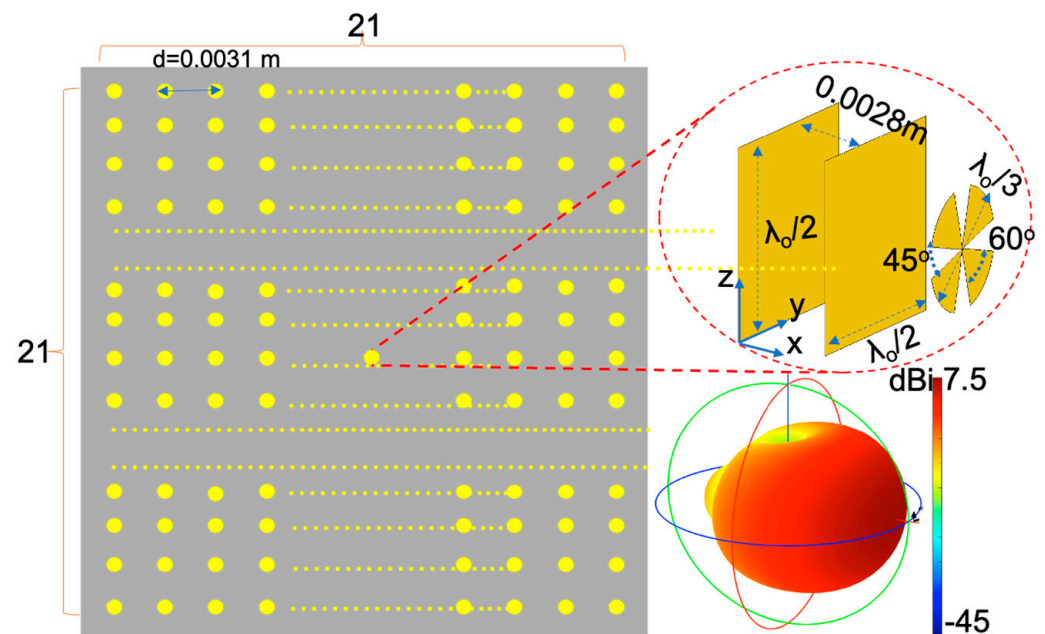


Figure 3. The proposed antenna array scheme of 21×21 REs (left panel) along with the geometry and the radiation pattern of each RE (right panel).

The formulation of all the electromagnetic characteristics of the current array scheme along with a multitude of radiation patterns has been thoroughly presented in our recent published work [29]. Hence, all the produced radiation diagrams as well as technical details about the REs are provided in every detail in the former published work. However, it is necessary to mention that all the antenna field properties have been calculated through the method of moments (MoM) [33], applied in a 3D computational model [34], which incorporates the deleterious effects of mutual coupling among REs. Thus, a realistic analysis of such type of antenna arrays has been carried out.

By using different phases for each RE in conjunction with the appropriate activation of either the entire array or a part of it (subarray), an efficient beamforming technique is adopted. Hence, such arrays increase the levels of manipulation of the radiation pattern. This allows the radiation pattern to be changed not only in terms of the desired direction (azimuth or elevation level) but also in terms of directivity [34]. As a result, a low-complexity beamforming technique is suggested together with an implicit steering mechanism. To this end, 51 different BCs can be formulated, including square and rectangular array configurations. Figure 4 provides an indicative example of the applied BCs, where multiple background colors have been used to distinguish among each other. In conclusion, adopting the proper array configuration necessitates the balancing of three distinct parameters: the number of the activated REs, the desired QoS and the required spatial coverage.

To this end, two representative scenarios explaining the mutual dependence of the aforementioned parameters are presented on the bottom right panel of Figure 4. Assuming that the required spatial coverage is defined between $+30^\circ$ and -30° , the current antenna array can accomplish this requirement with five configuration schemes, as shown in the table on the upper right panel of Figure 4. Supposing that the requested QoS requires an increased directivity, the most appropriate scheme would be 21×3 (63 REs), while a scenario characterized by a low QoS would require the activation of the 3×3 scheme (nine REs). Hence, a scenario with an even reduced required QoS could be facilitated by activating only one RE. Consequently, the main priority of the employed algorithm is to detect all the possible configuration schemes which ensure spatial coverage for all MSs of a sector. In turn, the algorithm decides which among them is the most efficient, in terms of power consumption, that accomplishes the demanded QoS.

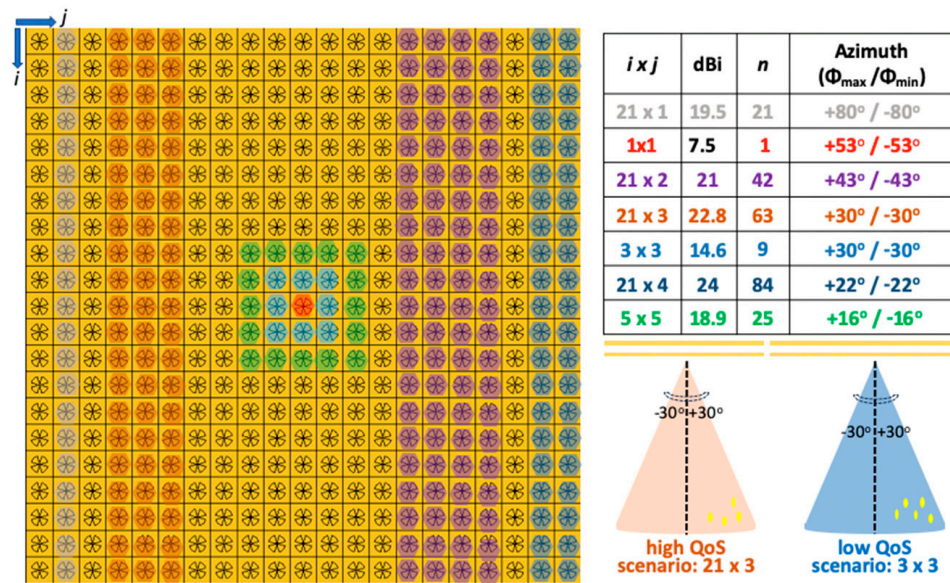


Figure 4. Representative antenna array configurations spotted with colors (left panel) in concert with their corresponding directivity in dBi, number of REs (n) and the azimuth coverage in degrees (Φ° , (upper right panel)) (a representative scenario employing different antenna array configurations for the same spatial coverage but with different services on demand is depicted at the (bottom right panel)).

4. Machine Learning Adaptive Beamforming Framework

In this section, the proposed ML adaptive beamforming framework is presented. A key advantage of the proposed approach is that it considers both SE and EE optimization during ML model training. In the first case, as in [29], the requested throughput in an active sector’s angular space is the input matrix, while the output is the configuration scenario. However, a disadvantage of this approach is that it could not capture channel and power variations. Hence, in this paper, we also consider EE during beamforming calculations. In this case, assuming that there are already accepted MSs in a sector, then the requested EE in this sector is updated according to the candidate MS, assuming that this MS can be served by the already existing configuration. If the entrance of this MS does not lead to power outage, then the output configuration remains the same. Otherwise, it is updated accordingly. In both cases, the input EE to the specific sector is calculated according to the previous state.

The proposed approach is described in Algorithm 1. The set $\mathcal{MS}_{b,s}$ indicates the accepted MSs in the s th sector of the b th BS, while the rejection flag (rf) indicates either the acceptance or rejection of the candidate MS. Moreover, index t_r indicates the current training sample (N_s samples in total) and matrix \mathbf{H}_k indicates the $M_r \times M_t$ channel matrix for the k th MS that has been calculated according to (2). Finally, W denotes the total system’s bandwidth, while $\mathbf{O}(m,n)$ is an $m \times n$ zero matrix. Each MS is assigned a specific number of physical resource blocks (PRBs) [35]. PRB and power allocation are performed with the help of functions $PRB_allocation$ and $power_allocation$, respectively. Note that MS rejection takes place in three cases: (1) PRB outage, (2) power outage for the specific MS, and (3) power outage for the b th BS (in the latter two cases, corresponding thresholds are defined by p_m/P_m , respectively). Moreover, if cases (1) and (3) take place, the Monte Carlo (MC) simulation comes to an end, as it will be described in Section 5 as well. If MS rejection is caused due to power transmission, then additional BCs are examined until their maximum limit is reached (N_{BC}).

The training matrices for both NNs (SE and EE) are denoted as \mathbf{X}_{SE} and \mathbf{X}_{EE} , respectively. Both matrices have size $N_s \times 180$, since each row entry represents the SE or EE distribution per sector’s angular space, as mentioned in Section 2. In **Step 6**, these training matrices are updated according to the SE or EE of the specific MS in angle φ_k :

$$SE_k(t_r, \varphi_k) = R_k/W \tag{6}$$

$$EE_k(t_r, \varphi_k) = R_k/P_k \tag{7}$$

Algorithm 1: ML-aided adaptive beamforming

Step 1: Initialization, $\mathcal{MS}_{b,s} \leftarrow \{\}$ ($1 \leq b \leq B, 1 \leq s \leq 3$), $t_r \leftarrow 0, k \leftarrow 0$
 $\mathbf{X}_{SE} \leftarrow \mathbf{O}(N_s, 180), \mathbf{X}_{EE} \leftarrow \mathbf{O}(N_s, 180)$

Step 2: $k \leftarrow k + 1$. The k th MS tries to enter the network in the s th sector of the b th BS at an angle φ_k requesting R_k Mbps ($rf \leftarrow 0$)

Step 3: $\mathcal{U}_k \leftarrow PRB_allocation(\mathbf{H}_k, R_k)$

Step 4: if ($|\mathcal{U}_k| \sim 0$) then $P_k \leftarrow power_allocation(\mathcal{U}_k, \mathbf{H}_k, BC(b, s))$
 else $rf \leftarrow 1$, Go to **Step 8**

(if $ML_mode == 0$)

Step 5: if $P_k > p_m$ or $\sum_{k' \in \mathcal{MS}_b} P_{k'} > P_m$ set $rf \leftarrow 1$. Then:
 while ($rf == 1$) and ($BC(b, s) < N_{BC}$)
 $BC(b, s) \leftarrow BC(b, s) + 1$
 $P_k \leftarrow power_allocation(\mathcal{U}_k, \mathbf{H}_k, BC(b, s))$
 if $P_k < p_m$ and $\sum_{k' \in \mathcal{MS}_b} P_{k'} < P_m$ then $rf \leftarrow 0$

Step 6: if ($rf == 0$) then $t_r \leftarrow t_r + 1$
 $\mathbf{X}_{SE}(t_r, \varphi_k) \leftarrow \mathbf{X}_{SE}(t_r, \varphi_k) + R_k/W, \mathbf{X}_{EE}(t_r, \varphi_k) \leftarrow \mathbf{X}_{EE}(t_r, \varphi_k) + R_k/P_k$
 $\mathbf{Y}_{SE}(t_r, 1) \leftarrow BC(b, s), \mathbf{Y}_{EE}(t_r, 1) \leftarrow BC(b, s)$
 if $|\mathbf{X}_{SE}(t_r, \cdot) - \mathbf{X}_{SE}(j, \cdot)| == \mathbf{O}(1, 180)$ or $|\mathbf{X}_{EE}(t_r, \cdot) - \mathbf{X}_{EE}(j, \cdot)| == \mathbf{O}(1, 180)$
 for $1 \leq j \leq t_r - 1$, then $t_r \leftarrow t_r - 1$
 else go to **Step 7**

Step 7: if ($t_r == N_s$) then $\text{NN}_{SE} \leftarrow train(\mathbf{X}_{SE}, \mathbf{Y}_{SE}), \text{NN}_{EE} \leftarrow train(\mathbf{X}_{EE}, \mathbf{Y}_{EE})$
 else

Step 5 (updated): $BC(b, s)_{SE} \leftarrow \text{NN}_{SE}(\mathbf{X}_{SE}), BC(b, s)_{EE} \leftarrow \text{NN}_{EE}(\mathbf{X}_{EE}), rf \leftarrow 0$
 $P_k \leftarrow power_allocation(\mathcal{U}_k, \mathbf{H}_k, BC(b, s)_{SE})$
 if $P_k > p_m$ or $\sum_{k' \in \mathcal{MS}_b} P_{k'} > P_m$ then
 $P_k \leftarrow power_allocation(\mathcal{U}_k, \mathbf{H}_k, BC(b, s)_{EE})$
 if $P_k > p_m$ or $\sum_{k' \in \mathcal{MS}_b} P_{k'} > P_m$ then
 $rf \leftarrow 1$
 Go to **Step 8**

Step 8: if ($rf == 1$) or $\sum_{k' \in \mathcal{MS}_{b'}} P_{k'} > P_m$ for the b' th BS ($1 \leq b' \leq B$), then MC simulation terminates,
 else Go to **Step 2**

As it is apparent from (6) and (7), the SE/EE of the k th MS is defined as the ratio of the MS's requested throughput to the total system's bandwidth/transmission power for the k th MS. Both networks are trained in **Step 7**, where the output configurations per system's state (i.e., row entry of $\mathbf{X}_{SE}, \mathbf{X}_{EE}$) are stored in matrices $\mathbf{Y}_{SE}/\mathbf{Y}_{EE}$. It should be noted at this point that in order to avoid data overlapping, there are no identical rows in both training matrices \mathbf{X}_{SE} and \mathbf{X}_{EE} . Therefore, the appropriate conditions have been added in the last two entries of Step 6.

When running the adaptive beamforming approach in ML mode (ML_mode flag equals 1), in a modified **Step 5**, for a new potential MS that tries to access the network, the updated SE and EE in this sector are calculated first. Hence, the appropriate BCs can now be defined with the help of the two previously trained NNs. If the output of the SE network leads to MS rejection, then the output of the EE network is examined as well.

Training samples aggregation is also depicted in Figure 5. Assuming similar MS distribution in all active BSs, then the state $\{\mathbf{S}_{b,s}, BC(b, s)\}$ for the s th sector of the b th BS (i.e., the spatial distribution of either the SE or EE) is sent to a central aggregator for model training. The output estimator is also sent back to all BSs of the orientation. In realistic 5G deployment scenarios, this central aggregator can be a mobile edge computing (MEC) server [20]. MEC, being a distributed approach, uses ML tools in heterogeneous topologies (such as 5G and 6G networks) to obtain CSI until the network's edges in order to define the resource allocation policy in each case. The goal of MEC is to minimize the computation time by allocating the traffic to different processing units. Therefore, once data are sent to the MEC server, training is allocated to the appropriate hardware elements to minimize the overall response times and thus the system's latency. Moving a step forward, FL approaches can be applicable as well. In this case, instead of centralized ML model training as depicted in Figure 5, training can be performed on localized MEC servers associated with specific BSs. Once local

training is finalized, the master model is periodically updated. In this way, convergence times can be improved. The required accuracy is achieved by multiple communication rounds between the server (central aggregator) and the edge devices, which train the model with their local datasets.

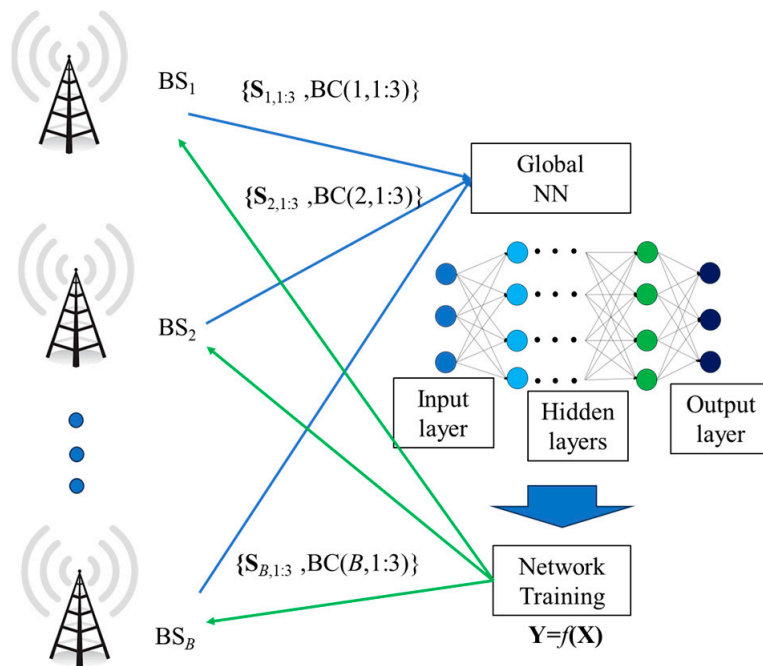


Figure 5. Training samples aggregation.

To train both networks, various numbers of hidden layers and neurons per layer were considered. In particular, calculations included one to five hidden layers and five to twenty neurons per layer. In all cases, the sample set was divided into two individual sets: a training set consisting of 70% of the individual samples as well as a validation set with the rest of the samples. The output metric in the training was mean square error (MSE). Therefore, the loss function can be defined as follows:

$$L(BC, BC_{est}) = \frac{1}{N_s} \sum_{i=1}^{N_s} (BC(i) - BC_{est}(i))^2 \tag{8}$$

where BC is the actual beamforming configuration defined in the non-ML network and BC_{est} is the corresponding estimation in ML mode. Both networks were trained with the help of the *trainlm* method using Matlab [34] (Levenberg–Marquardt backpropagation, [36]). As it can be observed from Figures 6 and 7, where indicative results are presented for 15 PBRs per MS (SE and EE, respectively), 5×5 networks were selected for both cases. In this context, the maximum allowed MSE was set to 0.9. The training outputs are the two NNs defined as NN_{SE} and NN_{EE} , respectively. Both networks take as input a particular spatial distribution of either SE or EE and provide an estimate of the appropriate BC.

Once both networks are trained, when running the simulation in ML mode, then the MS entrance is based on the SE network, as it was previously mentioned, since we cannot know a priori the optimum configuration for a specific sector. If the output of the SE network does not result in the acceptance of the new MS, then we examine the output of the EE network. A key advantage of this approach is that it can capture both channel and power variations. Rejection takes place only if both configurations cannot serve the new MS. It is important to note at this point that the approximation of the output configuration with NNs is a regression task. Hence, in all simulation scenarios, the output BC of either the SE network or the EE network is quantized with the round or with the ceil operator. Throughout the rest of this manuscript, the first method will be denoted as (R,R) while the second one will be denoted as (C,C).

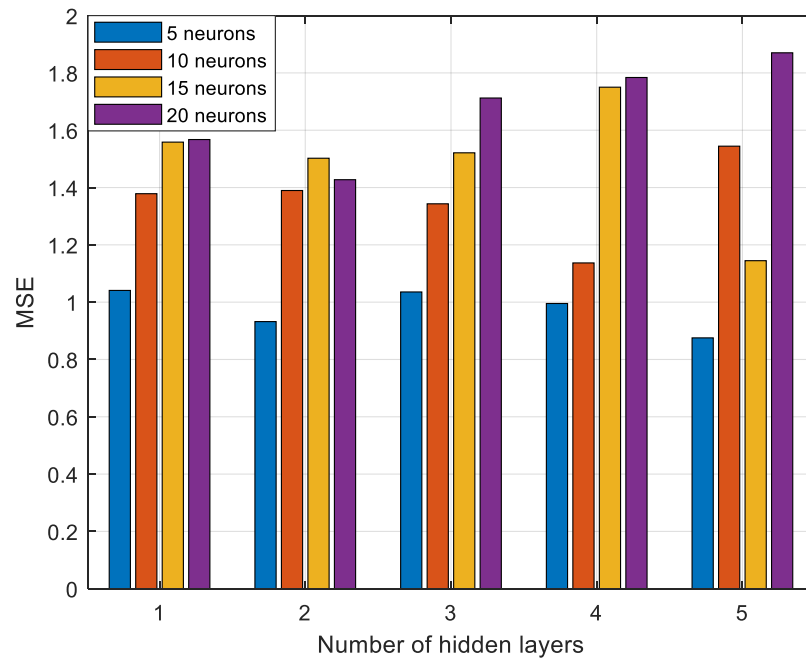


Figure 6. Mean square error for 15 PRBs per MS and SE training.

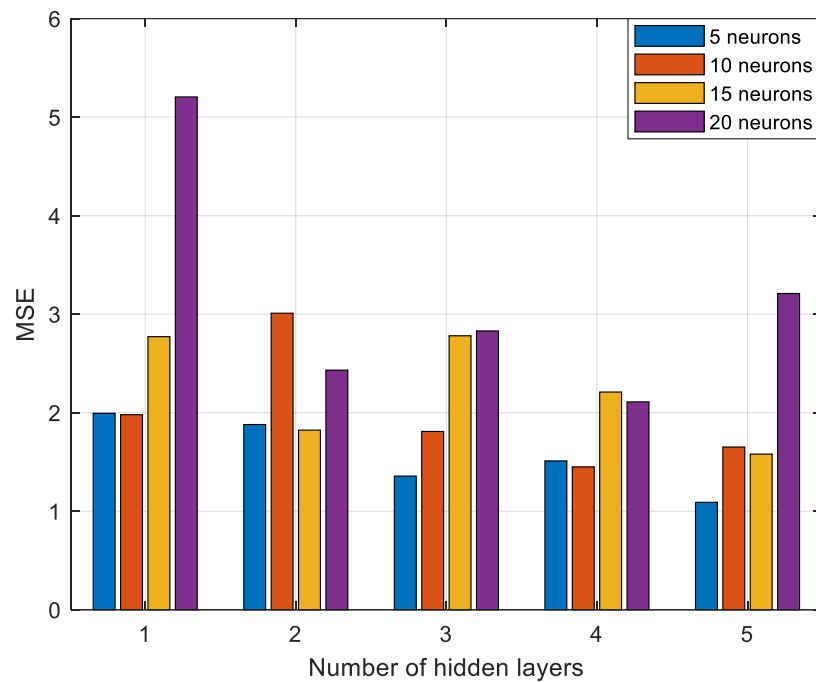


Figure 7. Mean square error for 15 PRBs per MS and EE training.

5. Simulation Setup and Results

All simulation parameters are summarized in Table 1. A carrier frequency of 28 GHz has been considered. It is assumed that MSs may request either five or 15 PRBs. Hence, requested throughput may vary from 7.2 to 21.6 Mbps (i.e., the product of PRBs per MS, subcarriers per PRB, subcarrier spacing, and bits per symbol for QPSK modulation). The cell radius equals 500 m, while hot spot areas are considered per BS in order to examine the performance of the proposed approach in highly demanding traffic scenarios. The performance of our proposed approach has been evaluated with the help of a developed system-level simulator that can execute MC simulations in parallel. The positions of the MSs as well as channel matrices remain constant during an MC run (semi-static simulator). For each scenario, 10^4 MC simulations were performed. The output KPIs are EE, SE, and REs as well as BP. All the aforementioned KPIs have been evaluated both for the non-ML/ML frameworks. A

typical MS distribution is shown in Figure 8, where an MS may be located in the hot spot area of a BS with a probability of 1/3.

Table 1. Simulation parameters.

Parameter	Value
Cell radius (m)	500
Carrier frequency (GHz)	28
Total bandwidth (MHz)	100
Pathloss model	UMa
Tiers of cells around the central cell/Number of cells	2/19
PRBs per MS	5/15
Modulation type per PRB	QPSK
Subcarrier spacing (kHz)	60
Subcarriers per PRB	12
PRBs per BS	132
Monte Carlo simulations per scenario	10^4
Required E_b/N_o (dB) for QPSK modulation [37]	9.6
Antenna elements per MS	2
Beamforming configurations (N_{BC})	51
Training samples per NN network	3000
Maximum power per BS/MS in W (P_m/p_m)	20/1

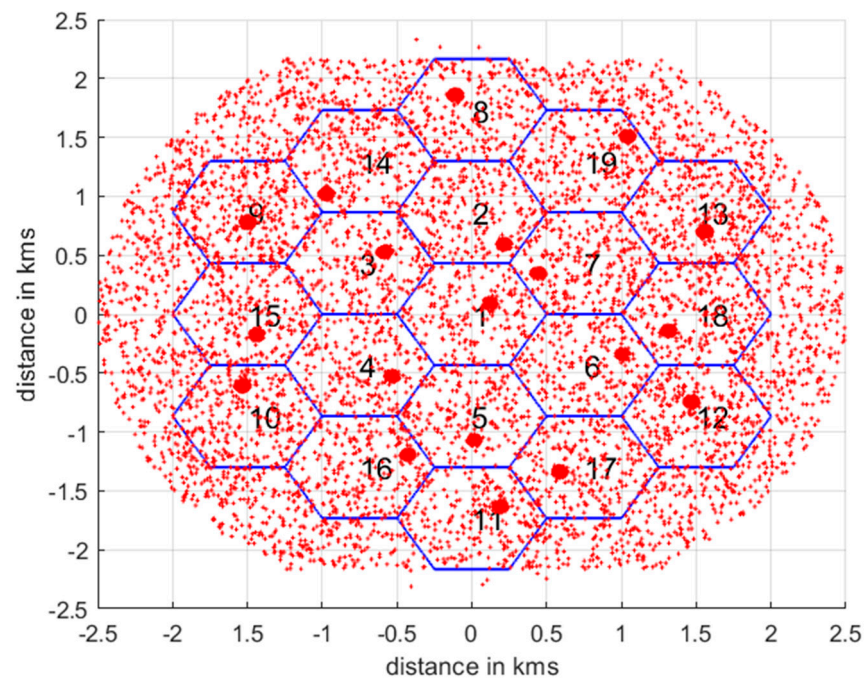


Figure 8. Non-uniform user distribution.

MSs enter the network sequentially, according to the predefined spatial distribution. For each candidate MS, all associated system-level parameters (e.g., pathlosses, shadowing, MIMO channel matrices) are calculated. In the non-ML mode, we examine whether the specific MS can be served by the already deployed configuration in a BS's sector. If this is the case, then the MS is admitted in the network, and all related parameters (i.e., transmission power per PRB/BS) are updated. Otherwise, additional BCs are examined, as described in Algorithm 1. MS rejection takes place only in the case where no BC can satisfy MSs' demands. The MC simulation comes to an end if the power of the PRB outage is triggered in at least one active BS, as explained in the previous section. Afterwards, all KPIs of interest are collected.

Simulation results are presented in Figures 9–12 (cumulative distribution function—CDF curves). In all cases, the standard non-ML approach has been considered as a reference basis along with the two ML assumptions per case. Throughout the rest of this manuscript, all output KPIs will

be compared with respect to their mean values. As it can be observed from Figure 9, where SE is presented, ML values are aligned with the non-ML ones. In particular, for five PRBs per MS, the corresponding SE is 16.5 bps/Hz. The corresponding value for 15 PRBs per MS is reduced to 13.3 bps/Hz. This reduction is rather expected, since in the latter case, fewer MSs are admitted in the network. It should be noted at this point that results come in agreement with the works in [38–40] (for the same number of transmitting elements) as well as with our previous work in [29].

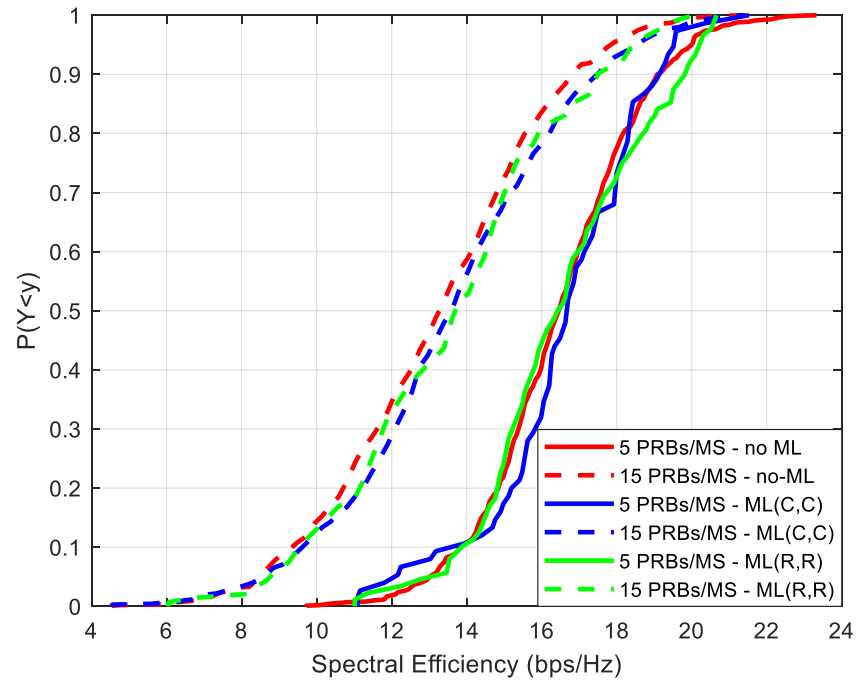


Figure 9. Spectral efficiency (bps/Hz).

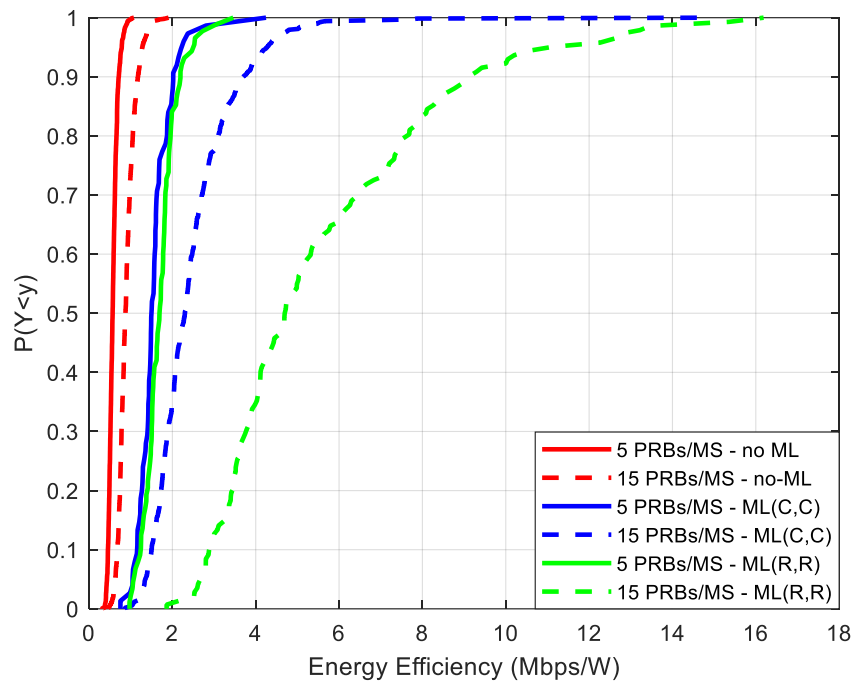


Figure 10. Energy efficiency (Mbps/W).

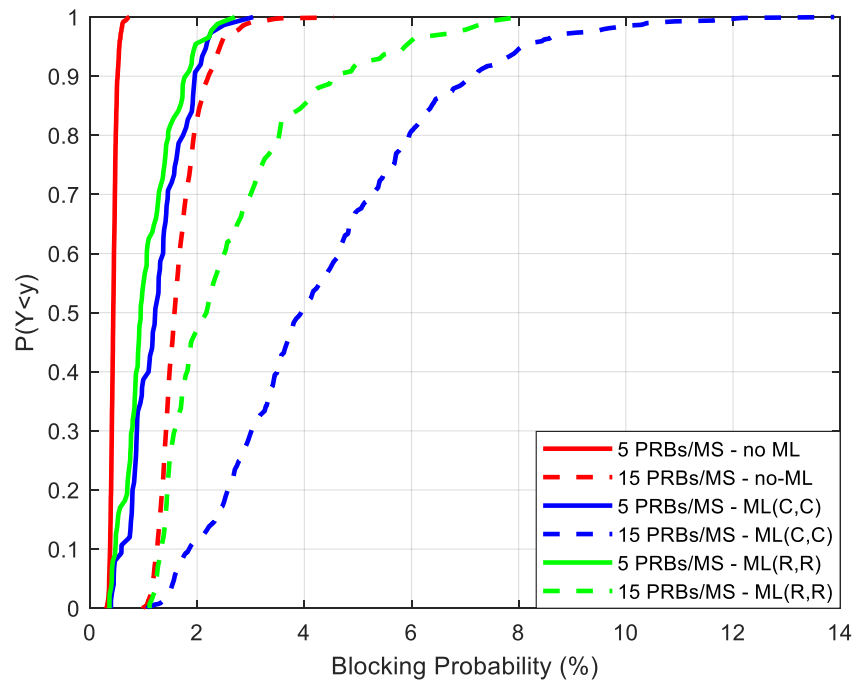


Figure 11. Blocking probability.

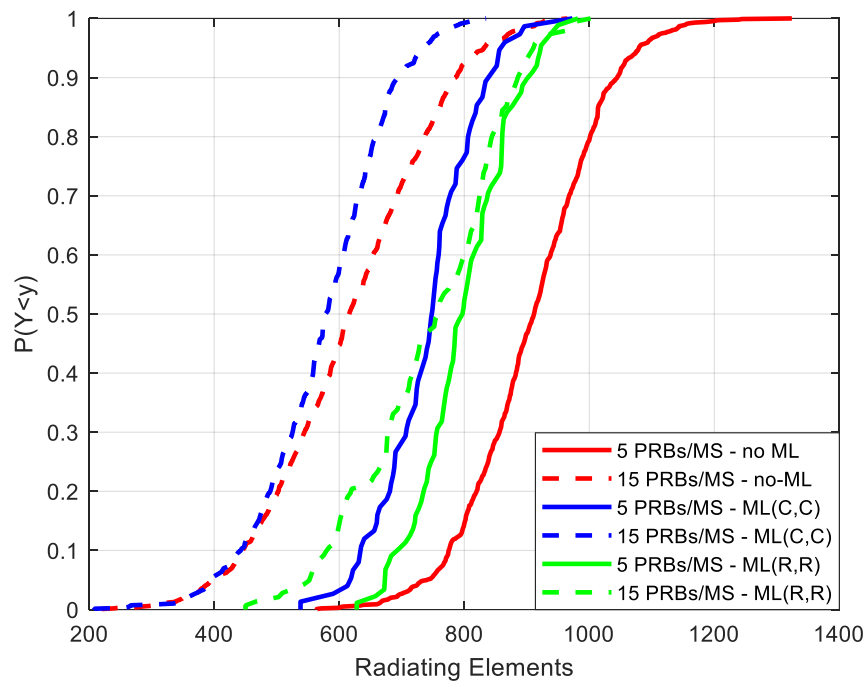


Figure 12. Radiating elements.

However, it is interesting to note from Figure 10 that both ML approaches can significantly improve the EE. In particular, for five PRBs per MS, when no ML is considered, the EE can reach up to 0.6 Mbps/W. The corresponding values for the (C,C) and (R,R) ML scenarios are 2.1/5 Mbps/W, respectively. For 15 PRBs per MS, the corresponding values are 0.9/2.5/5.3 Mbps/W for the non-ML/C-C/R-R scenarios, respectively. The aforementioned results come also in agreement with the work in [40] for the same number of transmitting antennas.

As it is apparent from Figure 12, where the total number of REs is depicted, this improvement may come with a reduced number of REs. In particular, for five PRBs per MS, there are 910 REs in the non-ML case. The corresponding values for the ML scenarios are 750/805 ((C,C) and (R,R) cases, respectively). For 15 PRBs per MS, the corresponding values are 620/575/750 for the non-

ML/ML(C,C)/ML(R,R) cases, respectively. Hence, improved EE comes at the cost of an almost 20% increase in REs. This amount, however, is significantly reduced compared to the corresponding EE improvement ratio (5.3 Mbps/W versus 0.9 Mbps/W, as previously mentioned).

As it can be derived from Figure 10, the EE is improved for 15 PRBs per MS. This improvement is more evident in the ML scenarios. In the non-ML case, the EE reaches 0.6/0.9 Mbps/W for 5/15 PRBs per MS, as previously mentioned. In this case, the appropriate BC is selected that provides an acceptable QoS to all MSs of a sector with the minimum number of REs, according to the analysis of Section 3. In the ML case, EE improvement among five and 15 PRBs per MS takes place as well due to the increased number of REs that formulate the specific BC. Hence, more narrow beams can now be configured, which unavoidably lead to an overall transmission power reduction.

It is interesting to note, however, from Figure 11 that BP can be significantly increased in the (C,C) scenario in both cases of PRB assignments per MS. In particular, for the standard non-ML scenario, then the corresponding BP values are 0.5/1.7% for 5/15 PRBs per MS, respectively. In the (R,R) scenario, the corresponding values are 1.1/2.6%, while in the (C,C) scenario, they are 1.29/4.36%, respectively. Hence, the BP increment is negligible in the ML (R,R) scenario for both cases of PRB assignments (5/15).

6. Conclusions

The performance of an adaptive beamforming approach for mmWave m-MIMO multicellular orientations has been evaluated via extensive system-level simulations. To this end, the goal was to reduce the complexity of beamforming calculations via ML. In particular, two neural networks were considered in order to predict the optimum configuration for a particular spatial distribution of the served users. The key novelty of the presented approach is that both spectral and energy efficiency were considered during neural network training. According to the presented results, for low data rate services, energy efficiency can be significantly improved with a reduced number of radiating elements compared to the standard non-ML approach. For high data rate services, although energy efficiency is again significantly improved, an additional number of radiating elements is required compared to the non-ML case. Even so, the corresponding increase in terms of percentage (i.e., 20%) is significantly reduced compared to the corresponding energy efficiency gain. In both cases, the increase in blocking probability is negligible.

In all cases of deviations from the standard non-ML framework, it becomes apparent that the proposed approach either underestimates (e.g., increased blocking probability) or overestimates (e.g., increased number of radiating elements) the appropriate beamforming configuration. Although a potential solution could be the incorporation of additional training samples or the deployment of additional training methods with stricter converge criteria compared to the Levenberg–Marquardt backpropagation method, these might increase the overall system's latency. In this context, a promising approach could be the deployment of deep reinforcement learning methods, since beamforming configurations are selected from a predefined discrete set of radiating elements. Therefore, instead of defining the appropriate beamforming configuration via regression methods which unavoidably introduce an estimation error, transitions among configurations could be defined according to the requested spectral or energy efficiency in a sector's angular space. The aforementioned approach is among others part of our future work.

Author Contributions: Conceptualization, S.L. and P.K.G.; methodology, P.K.G.; software, S.L.; validation, L.S., P.T. and K.P.; formal analysis, L.S.; investigation, E.T.; resources, S.L.; data curation, E.T.; writing—original draft preparation, P.K.G.; writing—review and editing, K.P.; visualization, P.T.; supervision, P.T.; project administration, P.K.G. All authors have read and agreed to the published version of the manuscript.

Funding: This research received no external funding.

Data Availability Statement: Data sharing not applicable.

Conflicts of Interest: The authors declare no conflict of interest.

References

1. Khan, B.S.; Jangsher, S.; Ahmed, A.; Al-Dweik, A. URLLC and eMBB in 5G industrial IoT: A Survey. *IEEE Open J. Commun. Soc.* **2022**, *3*, 1134–1163. [[CrossRef](#)]
2. Bockelmann, C.; Pratas, N.; Nikopour, H.; Au, K.; Svensson, T.; Stefanovic, C.; Popovski, P.; Dekorsy, A. Massive machine-type communications in 5G: Physical and MAC-layer solutions. *IEEE Commun. Mag.* **2016**, *54*, 59–65. [[CrossRef](#)]

3. Uwaechia, A.N.; Mahyuddin, N.M. A comprehensive survey on millimeter wave communications for fifth-generation wireless networks: Feasibility and challenges. *IEEE Access* **2020**, *8*, 62367–62414. [[CrossRef](#)]
4. Al-Dulaimi, O.M.K.; Al-Dulaimi, A.M.K.; Alexandra, M.O.; Al-Dulaimi, M.K.H. Strategy for non-orthogonal multiple access and performance in 5G and 6G networks. *Sensors* **2023**, *23*, 1705. [[CrossRef](#)]
5. Ibrahim, S.K.; Singh, M.J.; Al-Bawri, S.S.; Ibrahim, H.H.; Islam, M.T.; Islam, M.S.; Alzamil, A.; Abdulkawi, W.M. Design, Challenges and developments for 5G massive MIMO antenna systems at sub 6-GHz band: A Review. *Nanomaterials* **2023**, *13*, 520. [[CrossRef](#)] [[PubMed](#)]
6. Roy, D.; Salehi, B.; Banou, S.; Mohanti, S.; Reus-Muns, G.; Belgiovine, M.; Ganesh, P.; Dick, C.; Chowdhury, K. Going beyond RF: A survey on how AI-enabled multimodal beamforming will shape the NextG standard. *Comput. Netw.* **2023**, *228*, 109729. [[CrossRef](#)]
7. Wu, Q.; Zhang, R. Towards smart and reconfigurable environment: Intelligent reflecting surface aided wireless network. *IEEE Commun. Mag.* **2020**, *58*, 106–112. [[CrossRef](#)]
8. Liaskos, C.; Nie, S.; Tsioliariidou, A.; Pitsillides, A.; Ioannidis, S.; Akyildiz, I. A new wireless communication paradigm through software-controlled metasurfaces. *IEEE Commun. Mag.* **2018**, *56*, 162–169. [[CrossRef](#)]
9. Basar, E.; Di Renzo, M.; De Rosny, J.; Debbah, M.; Alouini, M.-S.; Zhang, R. Wireless communications through reconfigurable intelligent surfaces. *IEEE Access* **2019**, *7*, 116753–116773. [[CrossRef](#)]
10. Huo, Y.; Lin, X.; Di, B.; Zhang, H.; Hernando, F.J.L.; Tan, A.S.; Mumtaz, S.; Demir, Ö.T.; Chen-Hu, K. Technology trends for massive MIMO towards 6G. *Sensors* **2023**, *23*, 6062. [[CrossRef](#)]
11. Wang, J.; Zhang, X.; Shi, X.; Song, J. Higher spectral efficiency for mmWave MIMO: Enabling techniques and precoder designs. *IEEE Commun. Mag.* **2021**, *59*, 116–122. [[CrossRef](#)]
12. Mihaylova, D.; Valkova-Jarvis, Z.; Poulkov, V.; Stoykov, V.; Iliev, G. Investigation of hybrid beamforming in mmWave massive MIMO systems. In Proceedings of the 2020 IEEE 5th International Symposium on Smart and Wireless Systems within the Conferences on Intelligent Data Acquisition and Advanced Computing Systems (IDAACS-SWS), Dortmund, Germany, 17–18 September 2020; pp. 1–5. [[CrossRef](#)]
13. Dilli, R. Performance analysis of multi user massive MIMO hybrid beamforming systems at millimeter wave frequency bands. *Wirel. Netw.* **2021**, *27*, 1925–1939. [[CrossRef](#)]
14. Zhang, Y.; Wang, D.; Huo, Y.; Dong, X.; You, X. Hybrid beamforming design for mmWave OFDM distributed antenna systems. *Sci. China Inf. Sci.* **2020**, *63*, 192301. [[CrossRef](#)]
15. Imoize, A.L.; Obakhena, H.I.; Anyasi, F.I.; Sur, S.N. A review of energy efficiency and power control schemes in ultra-dense cell-free massive MIMO systems for sustainable 6G wireless communication. *Sustainability* **2022**, *14*, 11100. [[CrossRef](#)]
16. Zhou, A.; Wu, J.; Larsson, E.G.; Fan, P. Max-min optimal beamforming for cell-free massive MIMO. *IEEE Commun. Lett.* **2020**, *24*, 2344–2348. [[CrossRef](#)]
17. Enahoro, S.; Ekpo, S.C.; Uko, M.C.; Altaf, A.; Ansari, U.-E.-H.; Zafar, M. Adaptive beamforming for mmWave 5G MIMO antennas. In Proceedings of the 2021 IEEE 21st Annual Wireless and Microwave Technology Conference (WAMICON), Sand Key, FL, USA, 28–29 April 2021; pp. 1–5. [[CrossRef](#)]
18. Rekkas, V.P.; Sotiroudis, S.; Sarigiannidis, P.; Wan, S.; Karagiannidis, G.K.; Goudos, S.K. Machine learning in beyond 5G/6G networks—State-of-the-art and future trends. *Electronics* **2021**, *10*, 2786. [[CrossRef](#)]
19. Giannopoulos, A.; Spantideas, S.; Kapsalis, N.; Karkazis, P.; Trakadas, P. Deep reinforcement learning for energy-efficient multi-channel transmissions in 5G cognitive HetNets: Centralized, decentralized and transfer learning based solutions. *IEEE Access* **2021**, *9*, 129358–129374. [[CrossRef](#)]
20. Bartsiakos, I.A.; Gkonis, P.K.; Kaklamani, D.I.; Venieris, I.S. ML-based radio resource management in 5G and beyond networks: A survey. *IEEE Access* **2022**, *10*, 83507–83528. [[CrossRef](#)]
21. Gkonis, P.K. A survey on machine learning techniques for massive MIMO configurations: Application areas, performance limitations and future challenges. *IEEE Access* **2023**, *11*, 67–88. [[CrossRef](#)]
22. Tarafder, P.; Choi, W. Deep reinforcement learning-based coordinated beamforming for mmWave massive MIMO vehicular networks. *Sensors* **2023**, *23*, 2772. [[CrossRef](#)]
23. Vu, T.T.; Ngo, H.Q.; Dao, M.N.; Ngo, D.T.; Larsson, E.G.; Le-Ngoc, T. Energy-efficient massive MIMO for federated learning: Transmission designs and resource allocations. *IEEE Open J. Commun. Soc.* **2022**, *3*, 2329–2346. [[CrossRef](#)]
24. Liu, C.; Helgert, H.J. An improved adaptive beamforming-based machine learning method for positioning in massive MIMO systems. *Int. J. Adv. Eng. Technol.* **2020**, *13*, 1942–2652. Available online: http://www.ariajournals.org/internet_technology/ (accessed on 25 July 2023).
25. Aljohani, K.; Elshafiey, I.; Al-Sanie, A. Implementation of deep learning in beamforming for 5G MIMO systems. In Proceedings of the 2022 39th National Radio Science Conference (NRSC), Cairo, Egypt, 29 November–1 December 2022; pp. 188–195. [[CrossRef](#)]
26. Hassan, S.U.; Mir, T.; Alamri, S.; Khan, N.A.; Mir, U. Machine learning-inspired hybrid precoding for HAP massive MIMO systems with limited RF chains. *Electronics* **2023**, *12*, 893. [[CrossRef](#)]
27. Wu, X.; Luo, J.; Li, G.; Zhang, S.; Sheng, W. Fast wideband beamforming using convolutional neural network. *Remote Sens.* **2023**, *15*, 712. [[CrossRef](#)]

28. Son, W.; Han, D.S. Deep learning approach for improving spectral efficiency in mmWave hybrid beamforming systems. In Proceedings of the 2022 27th Asia Pacific Conference on Communications (APCC), Jeju Island, Republic of Korea, 19–21 October 2022; pp. 66–69. [[CrossRef](#)]
29. Lavdas, S.; Gkonis, P.K.; Zinonos, Z.; Trakadas, P.; Sarakis, L.; Papadopoulos, K. A machine learning adaptive beamforming framework for 5G millimeter wave massive MIMO multicellular networks. *IEEE Access* **2022**, *10*, 91597–91609. [[CrossRef](#)]
30. 3GPP TR 38.901 Version 14.3.0 Rel. 14, Study on Channel Model for Frequencies from 0.5 to 100 GHz, 2018. Available online: https://www.etsi.org/deliver/etsi_tr/138900_138999/138901/14.00.00_60/tr_138901v140000p.pdf (accessed on 25 July 2022).
31. Qu, S.; Ruan, C.-L. Effect of round corners on bowtie antennas. *Prog. Electromagn. Res.* **2006**, *57*, 179–195. [[CrossRef](#)]
32. Zheng, W.C.; Zhang, L.; Li, Q.X.; Leng, Y. Dual-band dual-polarized compact bowtie antenna array for anti-interference MIMO WLAN. *IEEE Trans. Antennas Propag.* **2014**, *62*, 237–246. [[CrossRef](#)]
33. Balanis, C.A. *Antenna Theory*, 4th ed.; John Wiley & Sons: Hoboken, NJ, USA, 2016; ISBN 978-1-118-64206-1.
34. *MATLAB*, version 9.11.0 (R2021b); MathWorks: Natick, MA, USA, 2021.
35. 3GPP TS 138 211, Version 15.3.0, Rel. 15, 5G NR Physical Channels and Modulation, 2018. Available online: https://www.etsi.org/deliver/etsi_ts/138200_138299/138211/15.03.00_60/ts_138211v150300p.pdf (accessed on 25 July 2022).
36. Lv, C.; Xing, Y.; Zhang, J.; Na, X.; Li, Y.; Liu, T.; Cao, D.; Wang, F.Y. Levenberg–Marquardt backpropagation training of multilayer neural networks for state estimation of a safety-critical cyber-physical system. *IEEE Trans. Ind. Inform.* **2018**, *14*, 3436–3446. [[CrossRef](#)]
37. Giuliano, R.; Monti, C.; Loreti, P. WiMAX fractional frequency reuse for rural environments. *IEEE Wirel. Commun.* **2008**, *15*, 60–65. [[CrossRef](#)]
38. Halbauer, H.; Weber, A.; Wiegner, D.; Wild, T. Energy efficient massive MIMO array configurations. In Proceedings of the 2018 IEEE Globecom Workshops (GC Wkshps), Abu Dhabi, United Arab Emirates, 9–13 December 2018; pp. 1–6. [[CrossRef](#)]
39. Zbairi, M.; Ez-zazi, I.; Arioua, M. Towards optimal spectral efficiency of cell free massive MIMO based linear detectors in 5G. In Proceedings of the 2020 International Symposium on Advanced Electrical and Communication Technologies (ISAECT), Marrakech, Morocco, 25–27 November 2020; pp. 1–6. [[CrossRef](#)]
40. Zhang, J.; Deng, H.; Li, Y.; Zhu, Z.; Liu, G.; Liu, H. Energy efficiency optimization of massive MIMO system with uplink multi-cell based on imperfect CSI with power control. *Symmetry* **2022**, *14*, 780. [[CrossRef](#)]

Disclaimer/Publisher’s Note: The statements, opinions and data contained in all publications are solely those of the individual author(s) and contributor(s) and not of MDPI and/or the editor(s). MDPI and/or the editor(s) disclaim responsibility for any injury to people or property resulting from any ideas, methods, instructions or products referred to in the content.